

PAPER • OPEN ACCESS

Recombinant spider silk membranes promote human renal epithelial differentiation and function

To cite this article: Alina Meyer *et al* 2026 *Biofabrication* **18** 025001

View the [article online](#) for updates and enhancements.

You may also like

- [Thin and stretchable extracellular matrix \(ECM\) membrane reinforced by nanofiber scaffolds for developing *in vitro* barrier models](#)
Jaeseung Youn, Hyeonjun Hong, Woojung Shin et al.
- [Standalone single- and bi-layered human skin 3D models supported by recombinant silk feature native spatial organization](#)
Savvini Gkouma, Nayanika Bhalla, Solène Frapard et al.
- [A study of the permeation and water-structuring behavioural properties of PEG modified hydrated silk fibroin membranes](#)
Aisling Mann, Fiona Lydon, Brian J Tighe et al.

Biofabrication



PAPER

OPEN ACCESS

RECEIVED

16 September 2025

REVISED

15 January 2026

ACCEPTED FOR PUBLICATION

28 January 2026

PUBLISHED

25 February 2026

Original content from this work may be used under the terms of the [Creative Commons Attribution 4.0 licence](#).

Any further distribution of this work must maintain attribution to the author(s) and the title of the work, journal citation and DOI.



Recombinant spider silk membranes promote human renal epithelial differentiation and function

Alina Meyer¹ , Lea-Maria Mayer¹ , Linnea Gustafsson^{2,3} , Jens Eriksson⁴ , Kathrin Klein⁵ , Florian A Büttner^{5,6} , Dinh Son Vo¹ , Madlen Hubert¹ , Volker M Lauschke^{5,6,7,8} , Mikael E Sellin^{4,9} , My Hedhammar¹⁰ and Per Artursson^{1,*}

¹ Department of Pharmacy, Uppsala University, Uppsala, Sweden

² Spiber Technologies AB, Stockholm, Sweden

³ Division of Micro and Nanosystems, KTH Royal Institute of Technology, Stockholm, Sweden

⁴ Department of Medical Biochemistry and Microbiology, Uppsala University, Uppsala, Sweden

⁵ Dr Margarete Fischer-Bosch Institute of Clinical Pharmacology, Stuttgart, Germany

⁶ University of Tübingen, Tübingen, Germany

⁷ Department of Physiology and Pharmacology and Center for Molecular Medicine, Karolinska Institutet and University Hospital, Stockholm, Sweden

⁸ Department of Pharmacy, The Second Xiangya Hospital, Central South University, Changsha, People's Republic of China

⁹ Science for Life Laboratory, Uppsala, Sweden

¹⁰ Division of Protein Technology, KTH Royal Institute of Technology, Stockholm, Sweden

* Author to whom any correspondence should be addressed.

E-mail: per.artursson@uu.se

Keywords: nanofibrillar membranes, recombinant spider silk, basement membrane, epithelial monolayer, epithelial differentiation, renal transport, endocrine disruption

Supplementary material for this article is available [online](#)

Abstract

Porous membranes are frequently used as supports of cell monolayers in functional studies of epithelial and endothelial barriers. However, commonly used conventional polymer-based membranes such as those made of polycarbonate (transwells) do not mimic the structural and biochemical properties of native basement membranes, which may limit cellular differentiation and function. Here, we use a nanofibrillar membrane that mimics the microenvironment of the basement membrane and is made of recombinant spider silk functionalized with the integrin-binding RGD motif of fibronectin and coated with human kidney-specific laminin-521 (FN-silk). The FN-silk membranes were evaluated as culture substrates for renal epithelial cells (RPTEC/TERT1), a cell type notoriously difficult to differentiate in culture. FN-silk membrane structure, cellular morphology, mRNA expression, barrier properties and transporter activity were assessed using scanning and transmission electron microscopy, RNA-sequencing, permeability and transport assays. Both FN-silk and conventional membranes supported barrier integrity and tight junction expression. In contrast to cultures on conventional membranes, the RPTEC monolayers on FN-silk exhibited a differentiated morphology, low expression of cell death markers, and, directional anion and cation transport. Further, the commonly used conventional membranes released endocrine-disrupting bisphenols that activated estrogen-mediated signaling. In summary, these findings indicate that FN-silk membranes with kidney-specific basement membrane laminin 521 reduces cellular stress, supports and maintains cellular differentiation and preserves important cellular functions. Our work establishes FN-silk membranes as a next-generation biomaterial that enables the differentiation of renal epithelial monolayers into a physiologically relevant *in vitro* model.

1. Introduction

Polarized epithelial cell monolayers representing different human tissues are in great demand for the

investigation of tissue-specific processes *ex vivo*. Often, these cultures are grown on porous membranes that promote differentiation by allowing nutrient access to both sides of the monolayer. Once

an intact monolayer has formed on such porous membranes, the directional transport of nutrients, toxicants and drugs across epithelial (e.g. intestinal, renal) or endothelial (e.g. blood–brain-barrier) monolayers can be investigated [1–3]. Cell monolayers grown on commercial porous membranes are therefore frequently used in both basic studies of cellular physiology and applied research including studies of drug transport. In addition, they can be used in more advanced co-culture formats, e.g. with a supporting layer of interstitial cells [4].

While epithelial cell barriers are attached to a tissue-specific basement membrane composed of fibrillar extracellular matrix (ECM) proteins *in vivo*, commercial porous membranes are made of artificial materials such as polycarbonate (PC), which can be coated with ECM proteins, to improve anchoring of sensitive cell types. Disadvantages of these conventional membranes include their thickness ($\geq 10 \mu\text{m}$), which can limit cell–cell communication between cells cultured on opposite sides of the membrane, and their stiffness, which negatively impacts the differentiation ability of epithelial cells [5]. Therefore, porous membranes that better mimic the native microenvironment are desirable.

The basement membrane, which surrounds and separates tissues and cell types, provides structural support for the cells. It consists of a thin but dense network of ECM protein fibrils with tissue-specific proportions of mainly collagens and structural glycoproteins such as laminin and fibronectin (FN), and associated proteoglycans [6]. In addition to providing structural support and other functions, the basement membrane plays a critical role in determining cell polarity [7]. In recent years, membranes made from recombinant spider silk proteins (spidroins) have emerged as a promising alternative to membranes based on synthetic polymers [8]. A specially engineered partial spidroin variant, 4RepCT [9], functionalized with the integrin-binding RGD motif of FN into FN-silk [10], self-assembles into thin (adjustable between 0.25–1.2 μm) but strong, elastic, biocompatible nanofibrillar membranes [8]. The FN-silk membranes have been shown to closely resemble the microenvironment of native basement membranes in terms of thickness [11], mechanical properties [11] and elasticity [8, 12]. They have previously been used to develop a variety of mono- and co-culture models of different cell types [11, 13–15]. Here, we extend these studies to a model of the renal proximal tubular epithelium, a cell type that is difficult to differentiate to physiological maturity using conventional *in vitro* setups. To further mimic the natural kidney basement membrane, the FN-silk membranes were coated with laminin-521.

We used the immortalized renal proximal tubular epithelial cell line RPTEC/TERT1, hereafter referred to as RPTEC, which forms tight junctions and domes

[16] and transports water [17], proteins [16] and cations [18, 19]. RPTEC cultures have been used in various formats for studies on renal epithelial barrier integrity [19, 20], ion transport [18, 19], nephrotoxicity [19, 21–25] and drug target identification (Meyer *et al* submitted to British Journal of Pharmacology 2025 [26]). However, RPTEC monolayers on conventional plastic-based membranes are not fully differentiated, limiting their applicability [24]. To improve differentiation RPTEC cells can be co-cultured with a supporting layer of immortalized fHDF/TERT166 fibroblasts, hereafter referred to as fibroblasts, which secretes soluble factors that promote epithelial differentiation [4].

Here, we explored whether differentiation of RPTEC renal epithelial cells could be improved when cells are cultured on FN-silk membranes, with or without a feeding layer of fibroblasts. Importantly, we found that when cultured on FN-silk, the RPTEC maintained a more native morphology and showed reduced cellular stress signaling including apoptosis compared to PC monolayer cultures. Barrier integrity and expression of cell junction proteins were preserved and RPTEC showed increased expression of several clinically relevant drug transporters and drug metabolizing enzymes as well as increased directional transport of anionic and cationic probe substrates. Furthermore, while estrogen signaling was perturbed by the release of the endocrine disrupting chemical (EDC) bisphenol A from PC membranes, estrogen signaling remained unaffected in FN-silk cultured cell monolayers. In summary, our results show that FN-silk monolayer cultures represent an incremental step towards a differentiated *in vitro* model of the human tubular renal epithelium.

2. Materials and methods

All materials and manufacturers are given in the supplementary file. Image analysis was performed in Fiji ImageJ (version 1.54p).

2.1. Preparation of membranes

FN-silk membranes were prepared as illustrated in figure 1(a), essentially as previously described [13]. Briefly, the FN-silk protein (FN-4RepCT, recombinantly produced in *E. coli*, purified using chromatography [9, 10]; 2 mg ml⁻¹ in PBS) was thawed at room temperature, transferred into a 48-well plate, and left overnight at room temperature for self-assembly into a membrane. A custom-made 3D-printed holder (Dental LT V2) was then lowered onto the membrane, allowing the membrane to attach around the holder within 2 h. After one hour of incubation, 3 $\mu\text{g ml}^{-1}$ of full-length recombinant human laminin-521 (BioLamina AB) was added for additional coating. After the 2 hr incubation,

the membrane was lifted, washed with Dulbecco's phosphate-buffered saline (DPBS) and transferred to a 24-well plate containing cell culture medium. Reproducibility of both FN-silk membrane formation and laminin-521 coating uniformity was verified through supplementary microscopy analyses using fluorescently labeled FN-silk and fluorescently labeled laminin-521, respectively. Polycarbonate (PC; 0.4 μm pore size, 10 μm membrane thickness, 24-well format) and polyethylene terephthalate (PET; 0.4 μm pore size, 12 μm membrane thickness, 24-well format) membranes were incubated overnight in cell culture medium, coated with 3 $\mu\text{g ml}^{-1}$ laminin-521 for 1 h and washed with DPBS before use.

2.2. Functional pore size analysis

To estimate the pore size of FN-silk membranes, fluorescent nanospheres (27 nm, 51 nm or 75 nm) were added to the apical side. At designated time points the membrane was removed from the well and the fluorescent intensity of the nanospheres in the receiving (basolateral) chamber was measured using a Spark microplate reader.

2.3. Cell culture

Immortalized renal epithelial cells RPTEC/TERT1 and immortalized human dermal fibroblasts fHD-F/TERT166 were purchased from Evercyte GmbH, Vienna, Austria. RPTEC cells were cultured in a 1:1 mixture of DMEM without glucose and Ham's F12, resulting in a final concentration of 5 mM glucose, and supplemented with 2 mM GlutaMAX, 5 $\mu\text{g ml}^{-1}$ bovine insulin, 5 $\mu\text{g ml}^{-1}$ transferrin, 10 ng ml^{-1} epidermal growth factor, 36 ng ml^{-1} hydrocortisone, 5 ng ml^{-1} sodium selenite, 100 U ml^{-1} penicillin and 100 $\mu\text{g ml}^{-1}$ streptomycin and 0.5% fetal bovine serum (FBS). Fibroblasts were expanded in DMEM/F12 (1:1) with glutamine and 1.2 g l^{-1} NaHCO_3 , supplemented with 10% FBS and 100 $\mu\text{g ml}^{-1}$ G418. For co-cultures, RPTEC cell medium was used as previously described [4]. RPTEC were seeded on the FN-silk membranes at a density of 140 000 cells cm^{-2} and fibroblasts onto the bottom of the 24-well plates at a density of 14 000 cells cm^{-2} . Fibroblasts were seeded 30 min prior to seeding of RPTEC to allow for cell attachment. The cells were cultured at 37 °C and 5% CO_2 , and the medium was renewed every 48–72 h. Experiments were performed 14 d after seeding to allow differentiation of RPTEC [4].

The culture formats used in this study are summarized in figure 1(b) and include RPTEC monolayers on FN-silk (Epi_{silk}), RPTEC monolayers on FN-silk with a fibroblast feeder layer (Epi_{silk}/F), RPTEC monolayers on PC (Epi_{PC}), RPTEC monolayers on PC with a fibroblast feeder layer (Epi_{PC}/F) and fibroblast monolayers (F). Unless otherwise specified, PC

membrane cultures served as controls. For experiments requiring optical transparency, such as bright-field and live-cell imaging, PET membrane cultures (Epi_{PET}/F) were used as references. These cultures were also included in the scanning electron microscopy SEM analysis of pore size and density and bisphenol release studies.

2.4. SEM

Epi_{silk}/F and Epi_{PC}/F cultures were fixed overnight at room temperature in 2% glutaraldehyde buffered with 0.1 M HEPES. After fixation, the samples were washed three times with 0.1 M HEPES buffer for 5 min each. Subsequently, serial dehydration was performed under agitation using 50%, 70% and 95% ethanol (two times for 10 min each), followed by 99.5% ethanol (three times for 15 min each). Samples were then serially dried with hexamethyldisilazane (HMDS), each step lasting 15 min: first with a 2:1 mixture of 99.5% ethanol and HMDS, then 1:1, followed by 1:2. Final drying was completed with three 15 min incubations in 100% HMDS. The remaining HMDS was allowed to evaporate overnight under a fume hood. The samples were then mounted on a conductive carbon tape and sputter-coated with a 12 nm thick gold layer using a PAK 600 coating system. Imaging was performed using a Zeiss Ultra 55 Gemini scanning electron microscope. Laminin-521-coated and uncoated FN-silk, uncoated PC and uncoated PET membranes without cells were mounted and imaged using the same protocol. Images of PC and PET membranes were converted to binary using the intermodes method (upper threshold set to 140) and the % area of black pixels was measured to determine porosity.

Additionally, the porosity for PC and PET membranes was calculated based on the manufacturer's specifications as

$$\text{Porosity (\%)} = \text{Pore density} * \pi r^2 * 100 \quad (1)$$

where r is the pore radius.

For porosity measurements of uncoated FN-silk membranes, they were lifted, placed in water overnight to remove PBS and dehydrated as described above. After drying, the FN-silk membranes were placed with either the apical or basal side up on carbon tape and coated with 5–9 nm gold using an MCM-100 table-top samples sputter. SEM and focused ion beam (FIB)-SEM were done using a Helios 5 UC. SEM images were acquired in the Immersion (UHR) mode with an acceleration voltage of 10 keV. Samples were etched using FIB at 30 keV for 3 s. Images were converted to binary using the intermodes method (upper threshold set to 40) and the Analyze Particles function was used to determine the pore area and number. Note that all particles less than 10 pixels² were excluded. The image-based

porosity was determined by counting the number of pixels occupied by the pores and dividing by the total area of the image. The pore radius r was calculated as

$$r = \sqrt{\frac{A}{\pi}} \quad (2)$$

where A is the measured pore area. The pore diameter was then obtained as $2r$.

2.5. Transmission electron microscopy (TEM)

Epi_{Silk}/F and Epi_{PC}/F cultures were washed once with DPBS. Samples were fixed in 2.5% glutaraldehyde buffered in 0.1 M Sorensen phosphate buffer pH 7.4 at room temperature for 1 h and then stored at 4 °C. The fixed samples were rinsed in 0.1 M phosphate buffer, followed by post-fixation in 2% osmium tetroxide in 0.1 M phosphate buffer, pH 7.4 at 4 °C for 2 h. The monolayers were then washed in 0.1 M phosphate buffer pH 7.4 and subsequently dehydrated stepwise in ethanol followed by acetone and finally infiltrated with resin and embedded in LX-112. Ultrathin sections (~80–100 nm) were prepared using an EM UC7 ultramicrotome, transferred onto formvar slot grids and contrasted with uranyl acetate followed by lead citrate. The grids were examined in a HT7800 transmission electron microscope at 80 kV and digital images were captured using a 20MPx Xarosa CMOS camera. Image analysis and scaling was performed in Fiji ImageJ and Affinity Designer (version 2.2.0).

2.6. RNA-seq

Epi_{Silk}, Epi_{Silk}/F, Epi_{PC}, Epi_{PC}/F and F cultures were washed once with DPBS. The FN-silk monolayers (Epi_{Silk}, Epi_{Silk}/F) were then scraped off, the PC monolayers (Epi_{PC}, Epi_{PC}/F) were cut out from the holder with an autoclaved blade and the basolateral fibroblasts (F) were scrapped off from the bottom of the well. Three to eight membranes were pooled and stored in 100 μl RNAlater. The samples were snap-frozen and stored at –80 °C until further processing. Total RNA was isolated using the Zymo Quick-RNA Microprep Kit including DNase treatment according to the manufacturer's instructions. Samples were processed using the NEBNext Ultra II Directional RNA Library Prep Kit (NEB #E7760S/L). Briefly, mRNA was isolated from total RNA using oligo-dT magnetic beads and fragmented. Subsequently synthesized cDNA was ligated to the sequencing adapters before amplification by PCR. Clustering and DNA sequencing were performed on a NovaSeqX plus instrument (Illumina) with a final loading concentration of 160 pM DNA at GenomeScan BV, Leiden, The Netherlands. Raw RNA-seq data were processed using the nf-core/rnaseq pipeline [27] (version 3.18.0). The data discussed in this publication have been deposited in NCBI's Gene Expression Omnibus [28] and are accessible through GEO Series accession

number GSE307014. Transcript expression was quantified by Salmon (version 1.10.3) with gene annotations from gencode (version 46). Genes with a minimum TPM > 1 across at least 2 samples were analyzed with the DESeq2 package [29] in R (4.3.1.). Count data were normalized by variance-stabilizing transformation. Gene set enrichments of Reactome pathways based on the normalized gene counts (p -value ≤ 0.05; multiple testing correction with the Benjamini–Hochberg method) were analyzed using clusterprofiler [30]. Cell proportions were determined by digital cytometry using CIBERSORTx [31] based on normalized gene counts, with Epi_{Silk} and F samples used as reference for RPTEC and fibroblasts, respectively. The experiments were performed with three replicates.

2.7. LC-MS/MS analysis of bisphenols

For the quantification of bisphenols (bisphenol A, bisphenol S, bisphenol B, bisphenol AF, bisphenol F, tetrabromobisphenol A), the cell culture medium was collected after overnight pre-incubation and after the last 48 h of the culture period. Epi_{Silk}/F, Epi_{PC}/F and Epi_{PET}/F cultures were washed twice with ice-cold DPBS, excised from the holders and pooled. Bisphenols were extracted from the cells by incubating them for 15 min at 500 rpm in 200 μl ice-cold acetonitrile (ACN)/water (60:40) with 50 nM warfarin as an internal standard. Culture medium samples were similarly diluted with warfarin-supplemented ACN to achieve the same concentrations. All samples were centrifuged at 3500 rpm for 15 min at 4 °C. Supernatants were analyzed by LC-MS/MS on a Waters Acquity UPLC coupled to a Waters Xevo TQ MS as previously described [32]. Values below the lower limit of quantification (S/N > 10) were excluded from further calculations. To determine the bisphenol concentration in the cells, the volume of a single RPTEC cell was estimated assuming a spherical shape with a diameter of 15 μm and multiplied by the total number of cells per membrane.

2.8. Permeability studies

To investigate the barrier integrity of Epi_{Silk}/F and Epi_{PC}/F cultures, the permeation of 50 μM Lucifer yellow (0.44 kDa) from the apical to the basolateral compartment was measured in the absence and presence of cells. The basolateral concentrations of Lucifer yellow were determined by fluorescence measurements in a Tecan Spark plate reader after 15, 30, 45 and 60 min. The apparent permeability coefficient (P_{app}) was calculated as

$$P_{app} = \frac{\Delta Q}{\Delta t} \frac{1}{AC_0} [\text{cm s}^{-1}] \quad (3)$$

where $\Delta Q/\Delta t$ is the permeability rate (in mol s^{–1}), C_0 is the initial concentration in the apical chamber

(in mol l^{-1}) and A is the surface area of the membrane (in cm^2).

The apparent resistance (R_{app}) was calculated as previously described [33]

$$R_{\text{app}} = \frac{1}{P_{\text{app}}} = \frac{1}{P_{\text{aq}}} + \frac{1}{P_{\text{c}}} + \frac{1}{P_{\text{f}}} \quad (4)$$

where P_{aq} is the permeability of the aqueous boundary layers adjacent to the apical surface and the basolateral surface of the filters, P_{c} is the permeability of the cell layer and P_{f} is the permeability of the filter membrane. P_{f} was calculated as described by Karlsson and Artursson [33], while P_{c} was calculated as the difference between the P_{app} of the membranes with cells and the P_{app} of the empty membranes. The reported cellular resistance (R_{c}), aqueous boundary layer resistance (R_{aq}), and filter resistance (R_{f}) correspond to the inverses of their respective permeability values. The experiments were performed with three to six replicates.

2.9. Immunofluorescence staining

Epi_{Silk}/F monolayers and fibroblasts cultured on FN-silk, respectively, were fixed with 4% paraformaldehyde, permeabilized with 0.1% saponin and blocked with 10% goat serum, each for 30 min at room temperature. Between each step, the cells were washed two to three times for 5 min each with DPBS. Primary and secondary antibody solutions were prepared in DPBS with 1% goat serum, 1% saponin, and 1% Triton-X 100. Primary antibodies used included anti-zonula occludens-1 (ZO-1, 1:100, monoclonal mouse), anti-SLC22A2 (OCT2, 1:200, polyclonal rabbit), anti-SLC22A6 (OAT1, 1:250, polyclonal rabbit) and anti-SLC22A8 (OAT3, 1:250, polyclonal rabbit). Alexa Fluor 488 (1:300, anti-mouse) and allophycocyanin (APC, 4 $\mu\text{g ml}^{-1}$, anti-rabbit) were used as secondary antibodies. Monolayers were incubated with the primary antibodies and then with the secondary antibodies for 1 h each at room temperature in the dark. The nuclei were stained with DAPI for 15 min before the monolayers were transferred to custom-made 3D-printed holders with coverslips. Finally, the mounting medium was applied and the samples were stored at 4 °C. Imaging was performed using a Leica Stellaris 5 confocal microscope equipped with a 40x/0.95 dry objective. The mean fluorescence intensity of the negative control (without primary, only with secondary antibodies) was subtracted from all respective images.

2.10. Anion transport studies

Epi_{Silk}/F or Epi_{PC}/F cultures were washed once with pre-warmed Hank's balanced salt solution (HBSS). The RPTEC monolayers were then incubated for 60 min with either HBSS or 100 μM probenecid in both compartments. After pre-incubation,

the solution was replaced with either 5 μM 6-carboxyfluorescein (6-CF) or 5 μM 6-CF with 100 μM probenecid in the apical (A–B) or basolateral (B–A) compartment. Samples were washed twice with ice-cold HBSS and lysed with 1% sodium dodecyl sulphate for 5 min. Fluorescence was measured in a Spark microplate reader ($\lambda_{\text{ex}} = 485 \text{ nm}$ and $\lambda_{\text{em}} = 535 \text{ nm}$) for six replicates for Epi_{Silk}/F and three replicates for Epi_{PC}/F cultures. The background fluorescence was subtracted and the relative fluorescence unit (RFU) was normalized to the surface area of the membrane.

2.11. Cation transport studies

Epi_{Silk}/F or Epi_{PET}/F cultures were washed once with pre-warmed HBSS. The monolayers were then incubated for 10 min with either HBSS or 50 μM of the OCT1-3 and P-gp inhibitor quinidine in both compartments [34–37]. After pre-incubation, the solution was replaced with either 10 μM 4-(4-(dimethylamino)styryl)-N-methylpyridinium iodide (ASP+) without or with 50 μM quinidine in the apical (A–B) or basolateral (B–A) compartment. Live cell imaging was performed using a custom-built microscope based on an Eclipse Ti2 body equipped with a 10X/0.45 Plan Apo Lambda air objective and a back-lit sCMOS camera with a physical pixel size of 11 μm (Prime 95B). The imaging chamber was kept at 37 °C and 5% CO₂ in a humidified atmosphere. Brightfield images were acquired using differential interference contrast (DIC), while fluorescence images were acquired using a 475/28 Spectra-X bandpass filter for excitation and a HQ610/75 nm filter for emission. Imaging was performed every 45 s for 30 min and five areas per monolayer were captured. Three monolayers were imaged for the main condition expected to represent functional transport ('ASP+', B–A'). Based on the good reproducibility observed between these replicates and given the complexity and time requirements of the imaging procedure, the remaining conditions were imaged in single replicates. Background fluorescence was subtracted from each image and quantification of ASP+ fluorescence was performed in Fiji ImageJ.

2.12. Statistics

Statistical analysis was performed in GraphPad prism (version 10.4.2). Results are presented as mean \pm SD unless stated otherwise. Statistical significance for RPTEC cell height was determined based on an unpaired t -test. For anion transport studies, statistical significance was determined with a one-way ANOVA followed by a Dunnett's multiple comparisons test compared to the 6-CF; B–A; FN-silk condition. For cation transport studies, statistical significance was determined based on a mixed-effects analysis followed by a Dunnett's multiple comparisons test compared to the ASP+; B–A condition.

3. Results

3.1. FN-silk membranes are highly porous

Based on our recent protein expression analysis and in partial agreement with previous reports, the laminin subunits α_5 , β_2 and γ_1 are among the most abundant in healthy human kidney tissue [38, 39]. In RPTEC cells, these isoforms are expressed in similar proportions, albeit at a lower overall abundance compared to tissue samples (figure S1). However, despite their clear presence in kidney tissue, the kidney-specific regulatory role of laminin-521 has not yet been fully characterized. Human recombinant laminin-521 was used to coat and functionalize both FN-silk membranes and PC or PET membranes which served as controls (figure 1(b)). While PC membranes are preferred due to their higher porosity (estimated from SEM images: 11%, calculated from the manufacturer's specifications: 12.6%; pore size: $0.4 \mu\text{m}$) which provides numerous pores per cell (figure S2), low porosity PET membranes (estimated from SEM images: 0.4%, calculated from the manufacturer's specifications: 0.3%; pore size: $0.4 \mu\text{m}$) are generally used for imaging due to their optical transparency. FN-silk membranes were prepared as described previously (figure 1(a)) [13]. Using SEM to investigate the pore area of FN-silk membranes, it was revealed that the porosity differs between the top surface and the volume of the membrane (figures 1(c)–(e)). The apical side of the membrane consists of an outermost dense layer with pores with a median area of $55 \pm 6 \text{ nm}^2$ (mean $93 \pm 15 \text{ nm}^2$) and a porosity of $11 \pm 1\%$ (table S1). In contrast, the basal side consisted of much larger pores with variable size, a median area of $85 \pm 16 \text{ nm}^2$ (mean $1714 \pm 414 \text{ nm}^2$) and a porosity of $48 \pm 3\%$ (table S1). Ion etching of the membrane confirmed that the porous structure was present throughout the bulk of the membrane (figure S3). Although the analysis was conducted on uncoated FN-silk membranes, additional SEM imaging revealed no morphological difference when membranes were coated with laminin-521 (figure S4).

From the SEM images it is apparent that the top layer, due to its smaller pores, serves as the rate-limiting barrier for the permeation of secreted factors, drugs or small particles through the FN-silk membrane. As drying the membrane for SEM analysis could affect its dimensions, we next aimed to approximate the pore size under wet cell culture conditions. Previous studies have shown that FN-silk membranes allow permeation of small molecules ($<4.6 \text{ nm}$), whereas particles larger than 100 nm do not pass through [8]. To further refine this threshold, we analyzed the permeation of fluorescent nanobeads in three different sizes (27, 51 and 75 nm). The 27 nm beads passed through the membranes within 1 h. In contrast, the 51 nm and 75 nm beads did not permeate

even after 48 h (figure 1(f)). This indicates that the pores in the membrane are larger than 27 nm , but smaller than 51 nm when wet, verifying that the pores shrank (to an 8.4 nm median diameter) during drying.

3.2. Renal epithelial cells grown on FN-silk membranes exhibit physiological cuboidal morphology

After 14 d in culture, the RPTEC cells showed a typical epithelial morphology in both Epi_{Silk}/F and Epi_{PET}/F culture formats when imaged with brightfield microscopy (figures 2(a) and (d)). Dome formation, a characteristic feature of 2D cultures indicating active water transport [16], was not observed in any case, suggesting unimpeded water flow across all membrane types. The FN-silk membrane was designed to be $1.6 \mu\text{m}$ thick (figure 2(b)), which is about eight times thinner than the PET membrane, and resulted in favorable optical properties and a higher resolution of the cell borders in the brightfield microscope (figures 2(a) and (d)). TEM images revealed that the RPTEC monolayers on both membranes expressed tight junctions, microvilli and a large number of mitochondria, a hallmark of healthy, differentiated RPTEC cells (figures 2(b) and (e)) [40]. The cells in the Epi_{Silk}/F culture were more cuboidal and not as spread out as in the Epi_{PC}/F culture with a mean cell height of $11.5 \pm 2.2 \mu\text{m}$ and $6.4 \pm 1.5 \mu\text{m}$, respectively (figure S5(a)). Notably, as the cell height measurements were based on samples prepared for TEM, a dehydrating method known to result in shrinkage [41], it can be assumed that cells in culture are even higher. Thus, these results align closely with dimensions of healthy proximal tubular cells *in vivo*, which are estimated to be $20.3 \pm 4.1 \mu\text{m}$ high [42]. SEM further confirmed the formation of an intact monolayer (figure S5(b)) and the presence of microvilli (Epi_{Silk}/F: $11 \pm 2 \text{ microvilli}/\mu\text{m}^2$; Epi_{PC}/F: $5 \pm 2 \text{ microvilli}/\mu\text{m}^2$) and individual primary cilia on the apical surface of RPTEC (figure S5(c)), consistent with previous reports [16, 43]. Cross-sectional imaging illustrates that the FN-silk membrane is very thin relative to the cell layer, in contrast to the much thicker PC membrane (figures (c) and (f)). Furthermore, ECM deposition by the renal epithelial cells was observed in Epi_{Silk}/F cultures but not in Epi_{PC}/F cultures (figures 2(c) and (f)).

3.3. RNA-seq reveals reduced cellular stress and intact nuclear hormone receptor signaling in cells grown on FN-silk membranes

To obtain an unbiased overview of the molecular phenotypes of the cultured cells on FN-silk and PC inserts, we used RNA-seq. As expected, we observed a clear difference in mRNA expression between renal epithelial cells (cultured in the different formats Epi_{Silk}, Epi_{Silk}/F, Epi_{PC}, Epi_{PC}/F) and fibroblasts (F)

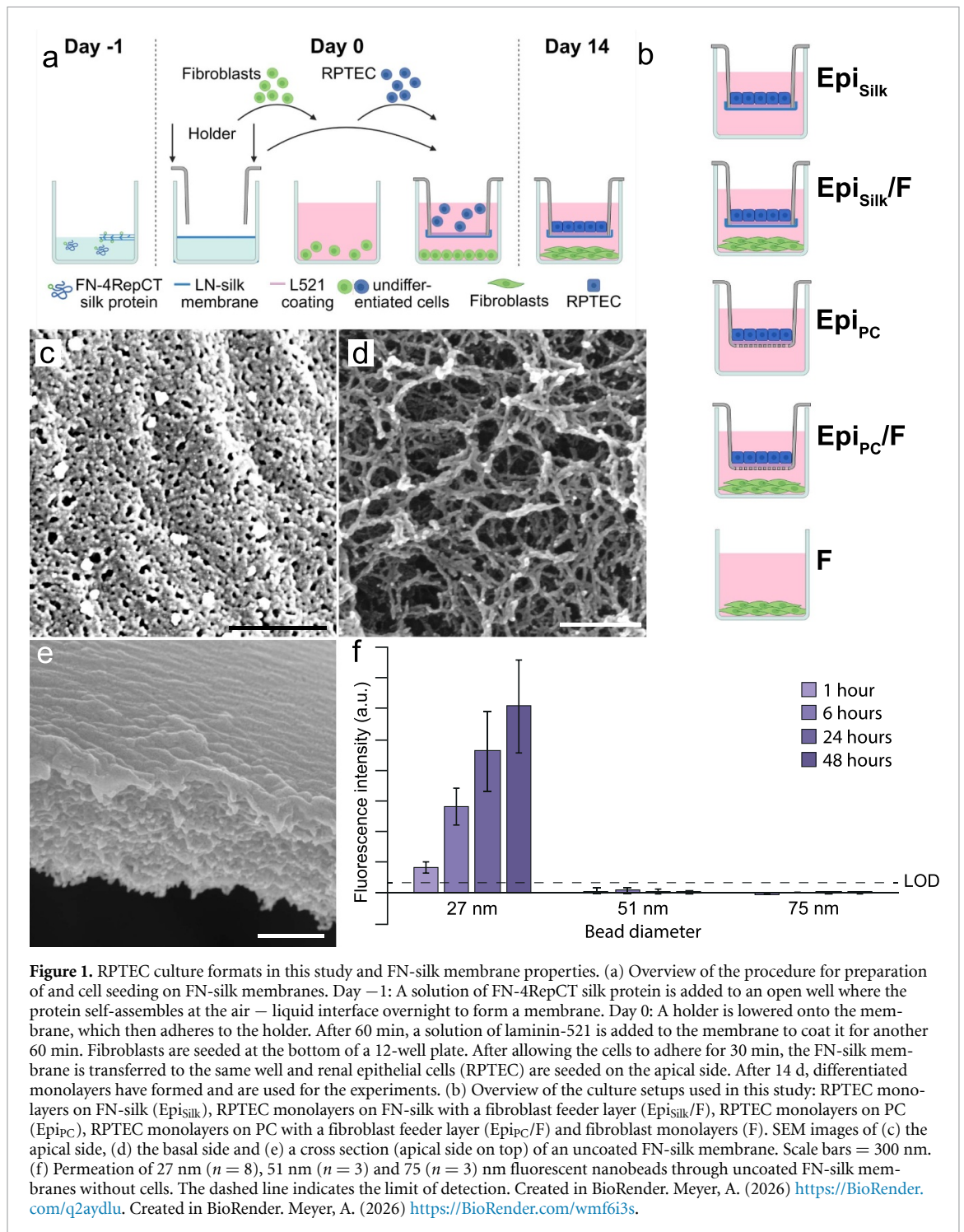


(figure 3(a), tables S2 and S3). Notably, transcripts of RPTEC cultured on FN-silk (Epi_{Silk} , Epi_{Silk}/F) and PC membranes (Epi_{PC} , Epi_{PC}/F) were largely clustered separately in an unsupervised analysis, indicating that the choice of membrane strongly impacts gene expression.

Digital cytometry identified signature genes for RPTEC and fibroblasts (table S4) and ensured that the RPTEC cells on the FN-silk membranes from the co-cultures (Epi_{Silk}/F) did not contain fibroblasts (figure 3(b)).

Next, we assessed the effect of adding fibroblast feeder layers. Fibroblast monocultures expectedly showed higher expression of genes involved in the organization of the ECM. In contrast, the renal epithelial cells showed higher expression of ADME (absorption, distribution, metabolism and excretion) genes and the barrier forming junctional complex (figures 3(c) and S6; table S5).

When comparing Epi_{Silk} and Epi_{Silk}/F cultures, the presence of feeder fibroblasts was associated with enhanced signaling via GPCRs and receptor tyrosine

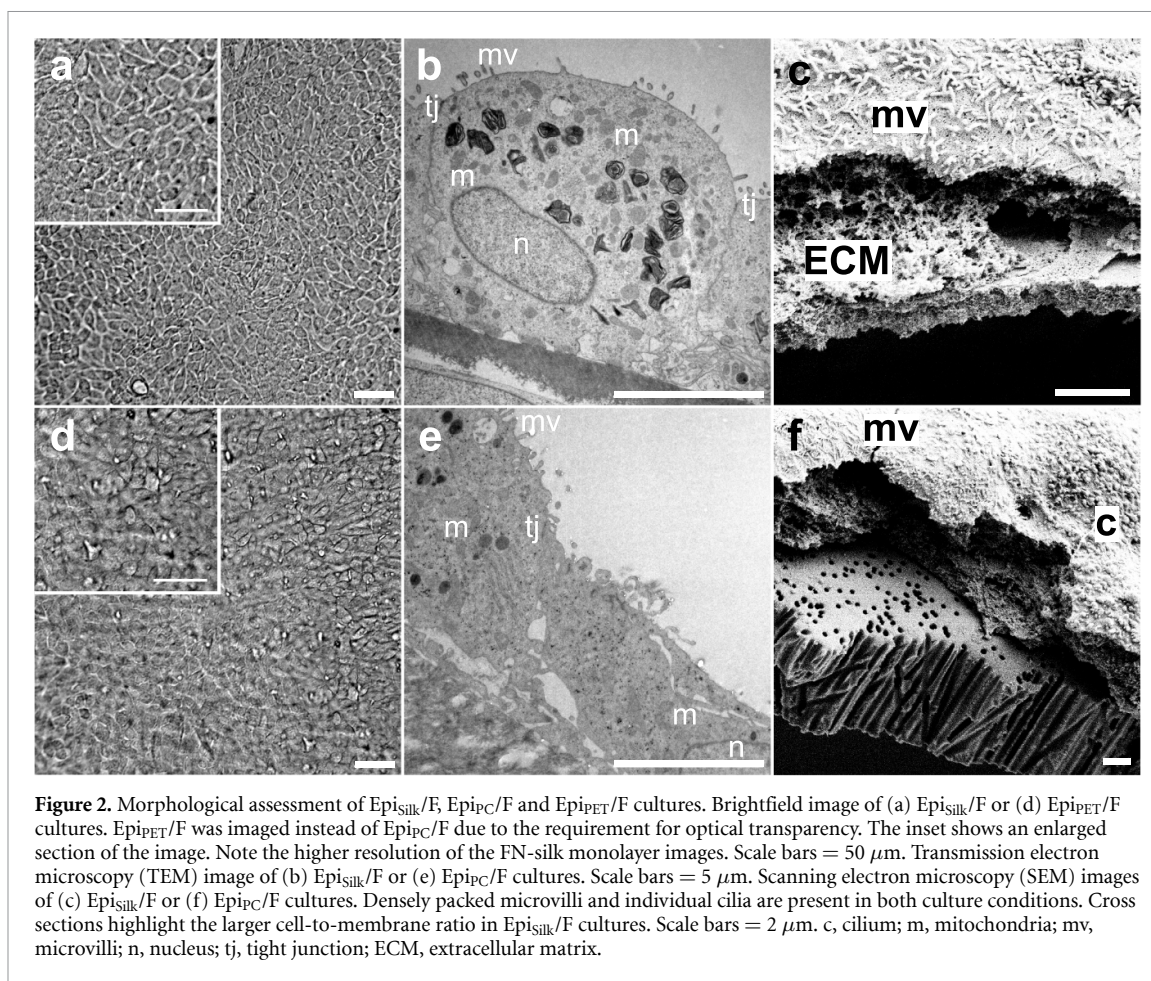


Figure 2. Morphological assessment of Epi_{Silk}/F, Epi_{PC}/F and Epi_{PET}/F cultures. Brightfield image of (a) Epi_{Silk}/F or (d) Epi_{PET}/F cultures. Epi_{PET}/F was imaged instead of Epi_{PC}/F due to the requirement for optical transparency. The inset shows an enlarged section of the image. Note the higher resolution of the FN-silk monolayer images. Scale bars = 50 μ m. Transmission electron microscopy (TEM) image of (b) Epi_{Silk}/F or (e) Epi_{PC}/F cultures. Scale bars = 5 μ m. Scanning electron microscopy (SEM) images of (c) Epi_{Silk}/F or (f) Epi_{PC}/F cultures. Densely packed microvilli and individual cilia are present in both culture conditions. Cross sections highlight the larger cell-to-membrane ratio in Epi_{Silk}/F cultures. Scale bars = 2 μ m. c, cilium; m, mitochondria; mv, microvilli; n, nucleus; tj, tight junction; ECM, extracellular matrix.

kinases along with the expected increase in ECM organization (figures S7 and S8; table S5). In contrast, Epi_{Silk} cultures showed higher levels of cell cycle checkpoint-related mRNA, indicating increased stress responses. Therefore, cultures with a support layer of fibroblasts were chosen for the subsequent experiments.

Several key proximal tubule markers (CUBN, ATP1A1, LRP2BP, GGT1, CLTC, ANPEP, DPP4) were expressed at similar levels in Epi_{Silk}/F and Epi_{PC}/F cultures (table S3). In contrast, aquaporin-1 (AQP1) and neprilysin (MME) showed reduced expression in Epi_{Silk}/F cultures relative to Epi_{PC}/F, whereas the proximal tubule endocytic receptor component amnionless (AMN), which partners with cubilin, was upregulated in Epi_{Silk}/F cultures (table S3). Additionally, Epi_{PC} cultures showed a more pronounced activation of immune response pathways, increased expression of cell death-associated caspases, and enhanced estrogen receptor signaling compared to Epi_{Silk} (figures 3(d)–(f) and S9; table S5). The latter was also observed in Epi_{PC}/F samples, suggesting potential leaching of EDCs from PC membranes. This is consistent with the known use of EDCs such as bisphenols in the production of PC, which may result in residual compound release [44]. Indeed, we detected $40.9 \pm 4.4 \mu$ M bisphenol A

(BPA) in the Epi_{PC}/F cultures, exceeding the reported EC₅₀ for estrogen receptor α activation in the MCF7 and ER α -CALUX assays [32]. This provides an explanation for the enhanced estrogen receptor signaling in these cultures. In contrast, the BPA levels in the culture medium remained below this threshold (figure 3(g)). No BPA was detected in Epi_{PET}/F cultures. Instead, bisphenol S (BPS) was detected in the preincubation culture medium from Epi_{PET}/F cultures but was not present in the samples collected during the later culture period (figure 3(h)). Whether the findings of significant levels of bisphenols are an inherent feature of all PC and PET membrane batches remains to be investigated. In contrast, none of the analyzed bisphenols (bisphenol A, S, B, AF, F or tetrabromobisphenol A) were detected in the Epi_{Silk}/F cultures, as expected, since these membranes are protein-based.

3.4. Renal epithelial cells on FN-silk membranes form intact barriers

In agreement with the TEM images, the transcriptomic data showed the expression of adherens and tight junction genes in all RPTEC cultures. Expression levels were overall higher in the Epi_{Silk}/Epi_{Silk}/F cultures than in the Epi_{PC}/Epi_{PC}/F cultures, particularly for cadherins (CDH) and claudins (CLDN)

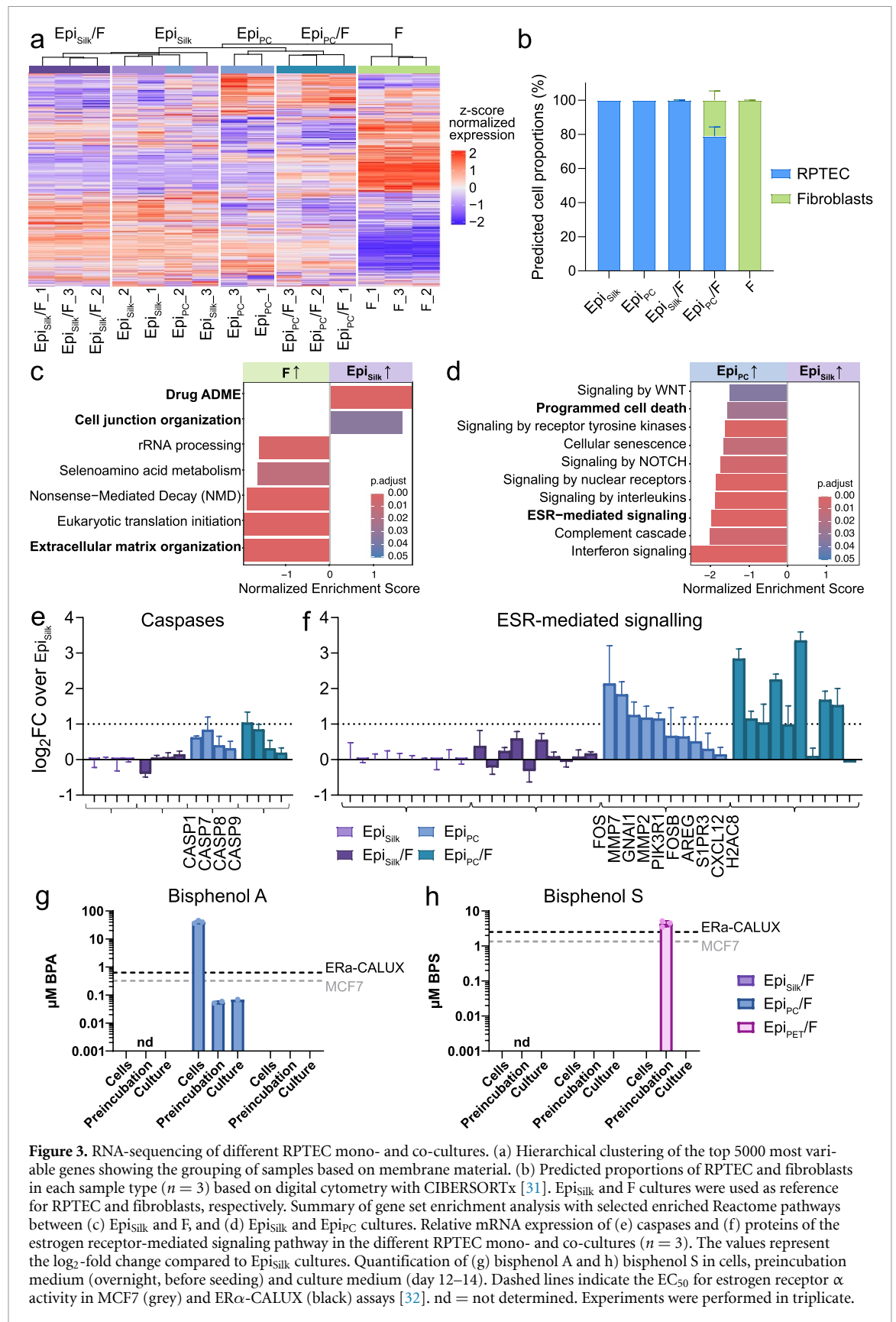


(figure 4(a)). The presence of an intact monolayer barrier in the Epi_{Silk}/F cultures was confirmed by the continuous expression of the tight junction protein 1/zonula occludens protein 1 (TJP-1/ZO-1) along the cell borders (figure 4(b)), consistent with

ultrastructural evidence of tight junctions by TEM (figure 2(b)). While immunostaining of additional junctional proteins could provide complementary information, it was not required to support the conclusions of this study. As adherens junction formation

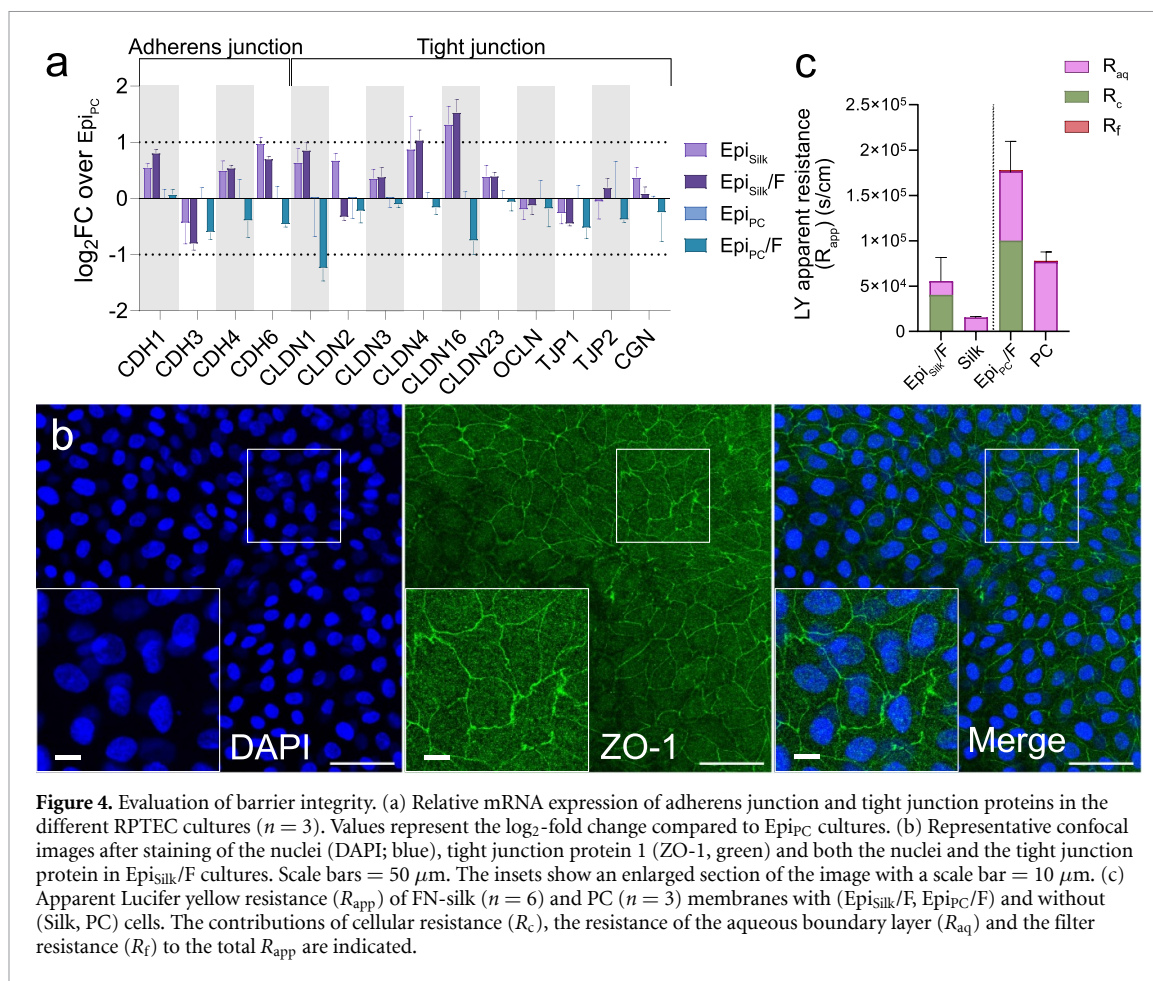


Figure 4. Evaluation of barrier integrity. (a) Relative mRNA expression of adherens junction and tight junction proteins in the different RPTEC cultures ($n = 3$). Values represent the \log_2 -fold change compared to Epi_{PC} cultures. (b) Representative confocal images after staining of the nuclei (DAPI; blue), tight junction protein 1 (ZO-1, green) and both the nuclei and the tight junction protein in Epi_{Silk}/F cultures. Scale bars = 50 μm . The insets show an enlarged section of the image with a scale bar = 10 μm . (c) Apparent Lucifer yellow resistance (R_{app}) of FN-silk ($n = 6$) and PC ($n = 3$) membranes with (Epi_{Silk}/F, Epi_{PC}/F) and without (Silk, PC) cells. The contributions of cellular resistance (R_c), the resistance of the aqueous boundary layer (R_{aq}) and the filter resistance (R_f) to the total R_{app} are indicated.

precedes tight junction formation, the observed continuous ZO-1 expression sufficiently supports barrier integrity.

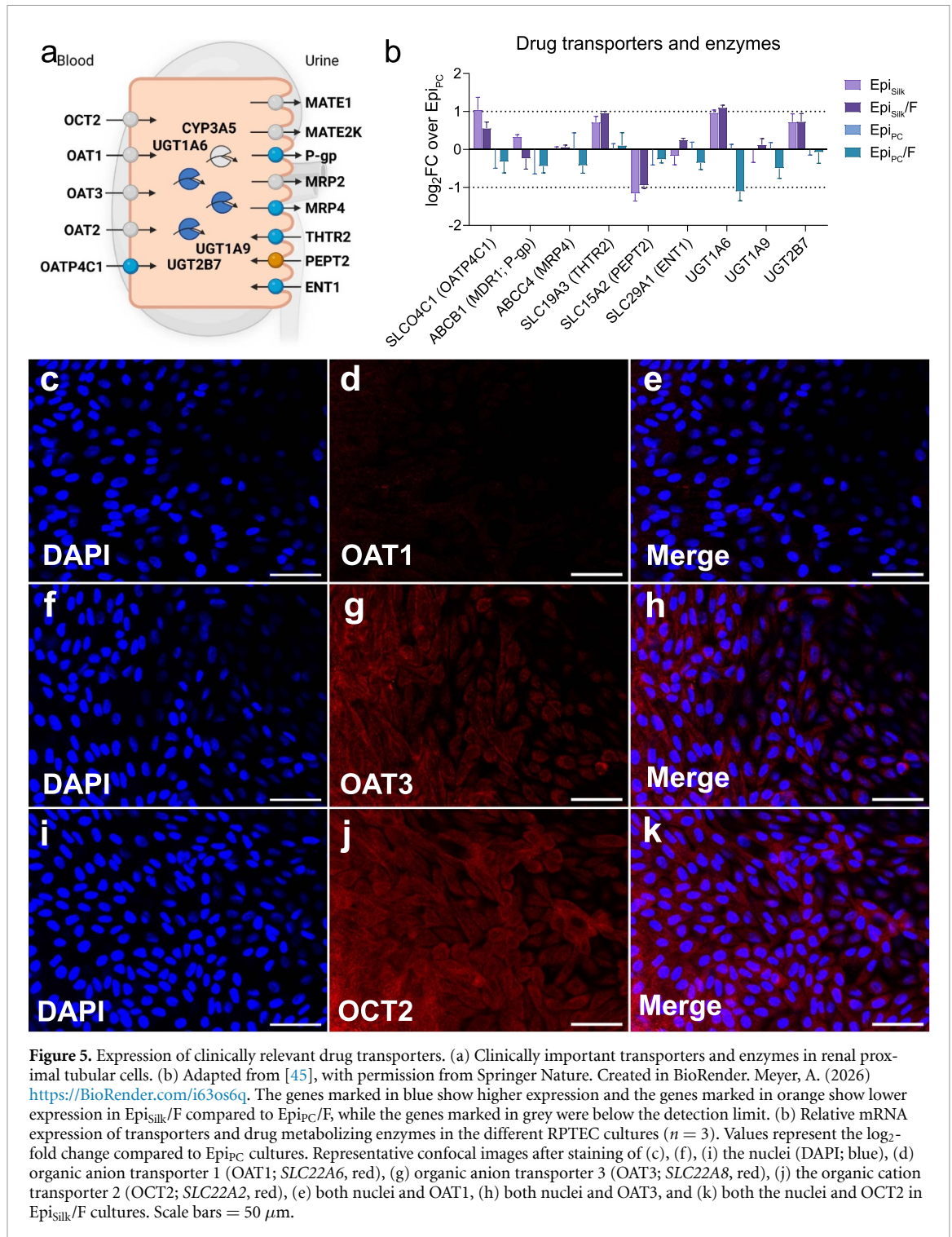
The apparent permeability of the hydrophilic probe Lucifer yellow (LY; 0.44 kDa) was then measured to further assess the barrier integrity of the RPTEC monolayers. Due to the delicate nature of the thin FN-silk membranes, stirring was not applied, so it was important to determine the contribution of the unstirred water layer to the total permeability of LY. This can be done by calculating the inverted permeability, i.e. the resistance. The total resistance to LY permeation (R_{app}) is the sum of the resistances of the filter membrane (R_f), the cell monolayer (R_c) and the aqueous boundary layer (R_{aq}) [33]. While R_f was negligible (0.3% of R_{app}), a significant contribution of the unstirred water layer to the overall resistance was observed for monolayers on both filters with a lower R_{aq} in Epi_{Silk}/F cultures (figure 4(c); table S6). This difference was probably caused by the different design and positioning of the two membranes, resulting in a thinner aqueous boundary layer in Epi_{Silk}/F cultures. The R_c differed about 2-fold between the cultures. Importantly, the apparent permeability of $5.6 \pm 1.2 \times 10^{-6} \text{ cm s}^{-1}$ determined in our Epi_{PC}/F cultures agreed with previous reports of primary and immortalized RPTEC cultures on

conventional 0.4 μm membranes, which ranged from 5.0 to $6.3 \times 10^{-6} \text{ cm s}^{-1}$ (table S7). Taken together, these results indicate that both types of membranes allowed the formation of intact monolayers with similar permeabilities.

3.5. Culture on FN-silk membranes enhances selective transport of both anions and cations

The barrier integrity of both RPTEC cultures allowed us to investigate renal transport function. Based on our RNA-seq results, most clinically relevant drug transporters and drug metabolizing enzymes had a higher expression in Epi_{Silk}/Epi_{Silk}/F than in Epi_{PC}/Epi_{PC}/F cultures (figures 5(a) and (b)). Further, immunofluorescence staining indicated the presence of some of the clinically most important drug transporting proteins in the basolateral membrane of the renal proximal epithelium, namely the anion transporter OAT3 (*SLC22A8*; but not OAT1, *SLC22A6*) and the cation transporter OCT2 (*SLC22A2*), in the Epi_{Silk}/F cultures (figures 5(c)–(k) and S10).

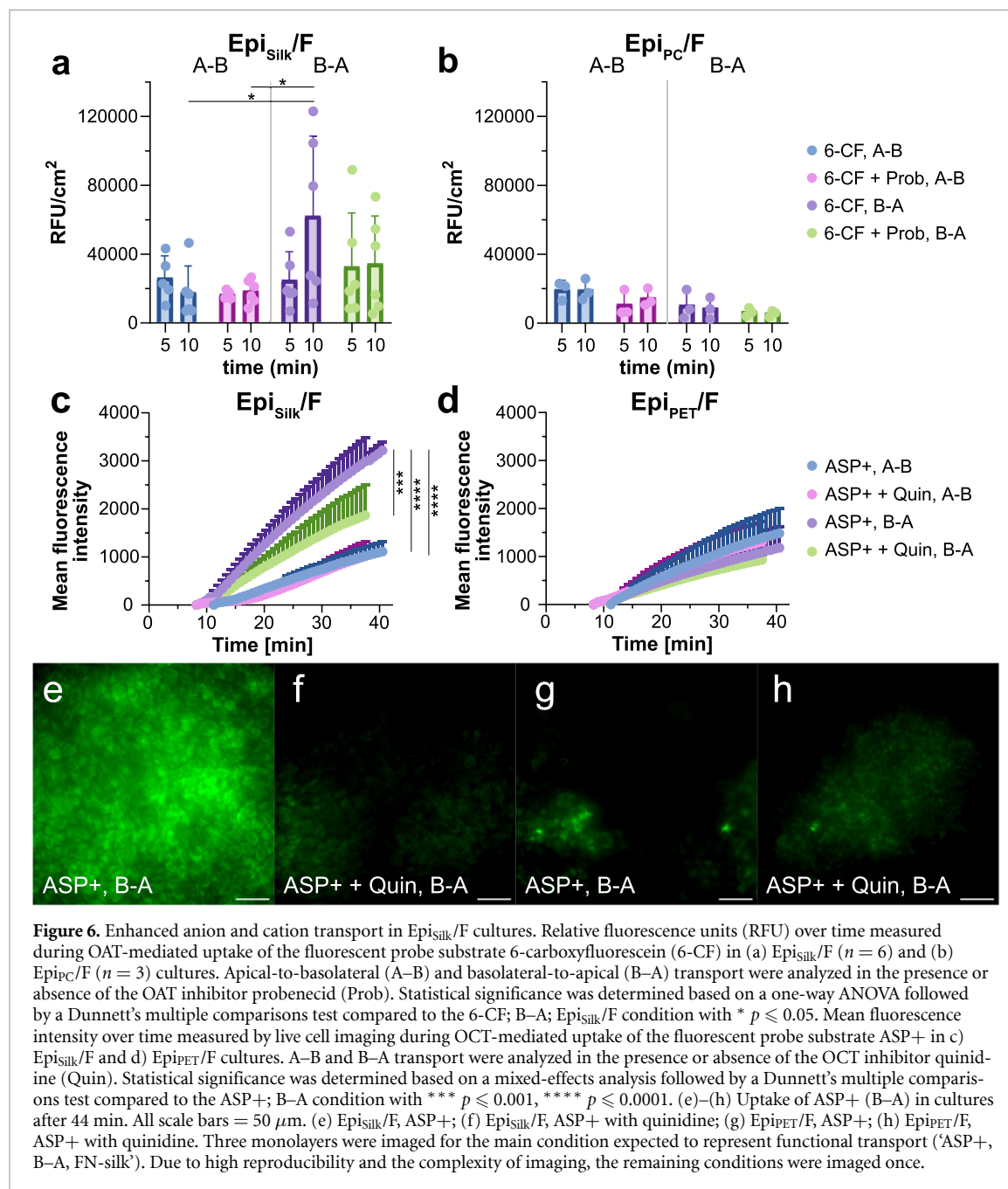
We therefore firstly investigated anion transport using the fluorescent probe substrate 6-carboxyfluorescein (6-CF). In Epi_{Silk}/F cultures, the 6-CF transport was significantly higher when the substrate was added to the basolateral compartment (B–A) than the apical compartment (A–B) (figure 6(a)).



Moreover, basolateral (B–A) 6-CF transport was inhibited by the OAT inhibitor probenecid [46]. In contrast, 6-CF transport was overall markedly lower, no significant differences in transport between A–B and B–A conditions, and no inhibition by probenecid were observed in Epi_{PC}/F cultures (figure 6(b)).

In parallel to our investigation of anion transport, we examined cation transport using the fluorescent probe substrate 4-(4-(dimethylamino)styryl)-N-methylpyridinium iodide (ASP+) and live cell

imaging. In Epi_{Silk}/F cultures, we observed significantly higher ASP+ transport in the B–A direction (figures 6(c) and (e)). This directional transport was effectively inhibited by the OCT inhibitor quinidine (figures 6(c) and (f)). Conversely, Epi_{PC}/F cultures showed no significant differences in ASP+ transport between the A–B and B–A directions, and quinidine had no inhibitory effect (figures 6(d), (g) and (h)). Together, our results show that the FN-silk membranes support the differentiation and polarized



transporter function of RPTEC, whereas no significant transport was observed in cultures on conventional membranes.

4. Discussion

In this study, we investigated FN-silk membranes as a novel substrate for renal epithelial monolayer cultures. RPTEC maintained on FN-silk obtained a more cuboidal morphology and showed reduced cell death and immune response signaling. Further, in contrast to cultures on conventional membranes, no baseline activation of estrogen-mediated signaling pathways was observed. The expression of several clinically relevant drug transporters and drug metabolizing

enzymes was higher in FN-silk monolayers and significant anion and cation transport was only observed in the latter. Thus, our results show that, relative to control membranes, FN-silk enhances the differentiation of renal epithelial cell monolayers toward a physiologically relevant *in vitro* model.

Since we found that the pore sizes of the FN-silk membranes are more than 7 times smaller than those of conventional membranes, we wondered whether this could hinder the diffusion of typical small molecule drugs. To assess this, we used the Stokes–Einstein equation to estimate the hydrodynamic diameter of three structurally diverse small molecules (salicylic acid, birinapant, bardoxolone methyl) that are currently being investigated for drug repurposing in the most common genetic kidney disease (Meyer

et al submitted to British Journal of Pharmacology 2025 [26]). All three molecules, as well as the probe substances LY, 6-CF and ASP+, have hydrodynamic diameters (0.7–1.2 nm) well below the nanobead permeability threshold of >27 nm. This indicates that small molecules can readily diffuse across FN-silk membranes. Consistent with this, the Renkin equation [47] yields a relative diffusion coefficient of approximately 0.85 for a representative small molecule ($\sim 500 \text{ g mol}^{-1}$; diameter $\sim 1 \text{ nm}$) diffusing through pores with a diameter of $\sim 27 \text{ nm}$, indicating only minor diffusion restriction. Thus, despite their smaller pore size, the thin FN-silk membranes provide close to unrestricted permeability to small drug-like compounds between the co-cultured cells.

Despite their advantages, FN-silk membranes posed some practical limitations. Their thin and elastic nature did require careful handling and we omitted stirring during transport assays as the membranes were prone to tearing, which affected experimental throughput. Increasing the thickness of the FN-silk membranes could overcome this limitation in future studies, although it may compromise some advantages of their thinness, while their strong support for cell attachment and elasticity would be preserved. Additionally, FN-silk membrane formation required overnight preparation and specialized inserts, which are currently not commercially available. However, a recently published step-by-step protocol now provides clear guidance for FN-silk membrane handling and 3D printing of the necessary inserts, making this system more accessible to the wider research community [13].

It is well known that sensitive cell types, including RPTEC cells, may not fully attach to polymeric membranes such as PC and PET, and this was also observed in our study. We addressed this issue by incubating the PC and PET membranes overnight in culture medium and additionally coating them with the kidney-specific laminin-521 prior to cell seeding. Notably, while our analyses identified laminin-521 as the most abundant laminin in human renal tissue samples, other commonly expressed isoforms, such as laminin-111 and laminin-511 or mixtures of kidney-specific laminins, can be investigated in future model refinements [39]. However, despite these coatings, the pipetting required during immunostaining still caused significant cell detachment from PC and PET membranes, rendering such experiments technically unfeasible. In contrast, the FN-silk membranes supported strong cell attachment. This is largely attributed to the RGD-containing cell-binding motif of FN, which promotes integrin-mediated binding. Interestingly, the integrin transcripts identified in our cultures (table S2) closely matched the corresponding proteins previously quantified in human kidney tissue [38], and their mRNA levels were comparable between FN-silk and PC conditions. This suggests

that the improved adhesion to FN-silk membranes was driven by the integrin-binding motifs rather than changes in cellular expression profiles, although the more physiologically relevant elasticity of the FN-silk membranes ($E \sim 115 \text{ kPa}$ [8]; human kidney tissue $E \sim 95\text{--}180 \text{ kPa}$ [12]), compared with the much stiffer track-etched membranes ($E \sim 1.9\text{--}2.9 \text{ GPa}$ [5]), may also have contributed.

Digital cytometry enabled the identification of distinct gene expression profiles characteristic of renal epithelial cells and fibroblasts (table S4) with the latter showing higher expression of genes involved in ECM organization, consistent with their physiological function [31, 48]. Remarkably, even after confirming the absence of fibroblasts in the Epi_{silk}/F culture samples (figure 3(b)), we observed an upregulation of the ECM organization pathway compared to epithelial monocultures (Epi_{silk}) (figure S7). This suggests that in addition to the increased secretion of ECM components already reported in 3D cultures on FN-silk [14], the presence of a fibroblast feeder layer further enhanced this response. Consistently, SEM imaging also showed increased deposition of ECM in Epi_{silk}/F cultures compared to Epi_{PC}/F cultures (figure 2(f)).

Surprisingly, we also observed an enrichment of the estrogen receptor signaling pathway in PC monolayers compared to FN-silk monolayers (figure 3(f)). This suggested the potential leaching of EDCs such as BPA from the PC membranes [44], which we were able to confirm. BPA-induced estrogenic signaling is known to activate several downstream pathways, including MAPK, PI3K/AKT and cAMP signaling, and can also induce nuclear transcription factors such as PPAR γ , C/EBPs and NRF2 [49]. Together, these factors influence important cellular processes such as growth, survival, proliferation, invasion and apoptosis. Consistent with these effects, we observed increased NRF2 expression in Epi_{PC}/F cultures compared to Epi_{silk}/F cultures. Bisphenol levels measured in cells on PC membrane and in medium from PET membrane cultures exceeded the EC₅₀ values that we reported in our recent study on estrogen receptor α activation by EDCs (figures 3(g) and (h)) [32]. Although the precise contribution of BPA to the enrichment of signaling pathways in RPTEC cultured on PC membranes cannot be fully determined here, the increased expression of caspases (figure 3(e)) supports the hypothesis that endocrine disruptors released from conventional porous membranes can alter the cellular transcriptomic fingerprint. Given the extensive use of PC and PET membranes in drug discovery and toxicology, our results indicate that the effects of bisphenol leaching should be considered in such studies.

The tight junction and adherens junction mRNA expression was increased in Epi_{silk}/F cultures (figure 4(a)). This included pore-forming claudins,

such as claudin-2 and -16, as well as barrier-forming claudins, such as claudin-1, -3 and -4 [50], and cell-cell adhesion-promoting cadherins. Overall, the identified junctional complex transcripts largely overlap with their protein counterparts that we recently quantified in human kidney tissues [38] indicating that immortalized RPTEC cultures on FN-silk recapitulate key features of the *in vivo* epithelial barrier complex. Despite the differences in mRNA expression, similar apparent permeabilities were observed for Epi_{silk}/F and Epi_{PC}/F cultures, also consistent with previous reports (table S7) [51–53]. To further increase the physiological relevance of cultures on FN-silk, the introduction of apical fluid shear stress should be considered. While primary cilia were already present under static conditions, the application of flow could further enhance epithelial polarization and cilia maturation [54]. However, the effect of applying shear stress on FN-silk membranes should first be investigated, since it might require thicker membranes and careful calibration to protect the integrity of the membrane. In this context, gentle rocking or shaking might be possible. Once optimized, agitation can also help to minimize the diffusional resistance caused by the aqueous boundary layer [33].

Our transcriptome analysis also revealed the expression of clinically relevant drug transporters essential for active renal reabsorption and secretion of larger, hydrophilic and charged molecules, including many drugs. Key transporters include the basolateral OAT1/3 and OCT2 as well as the apical multidrug and toxin extrusion proteins MATE1 and MATE2-K [45]. All of these are critical for drug disposition in renal proximal tubular epithelial cells and represent common sites of clinically significant drug-drug interactions or drug-induced nephrotoxicity. Regulatory guidelines therefore recommend *in vitro* assessment of whether investigational drugs are substrates of these transporters [55]. To demonstrate the enhanced differentiation achieved in our FN-silk system, we limited our analysis to the basolateral uptake transporters, which typically show low mRNA expression in conventional porous membrane cultures [24]. Using immunofluorescence staining, we confirmed the expression of OAT3 (figure 5(g)) and OCT2 (figure 5(j)) in Epi_{silk}/F cultures. While some previous studies have demonstrated directional ASP⁺ transport in RPTEC/TERT1 grown on conventional membranes, directional transport of 6-CF has not been reported in this model [18, 19, 51]. In contrast, we observed significant directional anion and cation transport across FN-silk monolayers, whereas cultures on conventional PC and PET membranes showed no such transport (figure 6), highlighting an important advantage of the FN-silk membranes. Notably, mRNA expression of other renal transporters, such as the water-transporting aquaporins, remained constant across all tested conditions,

suggesting that their expression is less dependent on the culture substrate.

5. Conclusion

In summary, we demonstrated that co-culturing RPTEC renal epithelial cells with a supportive layer of fibroblasts on FN-silk membranes resulted in a cell morphology that more closely resembles the mature proximal tubular epithelium. Unlike cultures on conventional porous membranes, which showed activation of estrogen-mediated signaling pathways triggered by EDCs, FN-silk monolayers exhibited less cellular stress responses and no such activation. Barrier integrity was maintained and the essential directional uptake of anions and cations via clinically relevant drug transporters was restored. We tentatively conclude that the renal epithelial *in vitro* system on FN-silk membranes presented here opens up exciting possibilities for transporter research and co-culture with other cell types, e.g. endothelial cells, primary cells, or development of disease-relevant kidney models [11, 56, 57]. Our work highlights the potential of FN-silk as a next-generation biomaterial that enables physiologically relevant renal *in vitro* models for both basic and applied biomedical research.

Acknowledgments

This work was supported by the Swedish Research Council grant for Per Artursson (2017-01951) and My Hedhammar (2022-04209). The live-cell imaging infrastructure has been enabled by funds from the SciLifeLab Fellows program to M E Sellin. Volker M Lauschke and Kathrin Klein acknowledge support from the Robert Bosch Foundation, Stuttgart, Germany. Volker M Lauschke also acknowledges support from the ERC Consolidator Grant 3DMASH [101170408] and the Swedish Research Council [2021-02801, 2023-03015 and 2024-03401].

The authors would like to acknowledge the EMil core facility financed by the Infrastructure Board at Karolinska Institutet for providing assistance in transmission electron microscopy. The BioVis platform of Uppsala University was used to conduct experiments using the Leica Stellaris 5 confocal microscope. The authors would like to thank Spiber Technologies AB for kindly providing the FN-silk protein, BioLamina AB for providing LN521, and Mona Widhe for the deliveries. The authors also thank Igor Liebermann at Dr Margarete Fischer-Bosch Institute of Clinical Pharmacology for help with RNA isolation and quality measurements. Furthermore, the authors would like to thank Dr Evgeniya Mickols for her support with the LC-MS/MS analysis.

Figures 1(a) and (b) (<https://BioRender.com/p6mik7t>) and 5(a) (<https://BioRender.com/i63os6q>) created in BioRender. Meyer, A. (2025).

Data availability

The data that support the findings of this study are openly available at the following URL/DOI: <https://www.ncbi.nlm.nih.gov/geo/query/acc.cgi?acc=GSE307014>.

Supplementary Data available at <http://doi.org/10.1088/1758-5090/ae3eb9/data1>.

Table S2 available at <http://doi.org/10.1088/1758-5090/ae3eb9/data2>.

Table S3 available at <http://doi.org/10.1088/1758-5090/ae3eb9/data3>.

Table S4 available at <http://doi.org/10.1088/1758-5090/ae3eb9/data4>.

Table S5 available at <http://doi.org/10.1088/1758-5090/ae3eb9/data5>.


Conflict of interest


L G works for and M H has shares in Spiber Technologies AB, the company that produces the FN-silk protein. V M L is co-founder, CEO and shareholder of HepaPredict AB, as well as co-founder and shareholder of Shanghai Hepo Biotechnology Ltd.


Declaration of generative AI and AI-assisted technologies in the writing process


During the preparation of this work the author(s) used OpenAI's ChatGPT in order to improve the clarity and readability of the manuscript. After using this tool/service, the author(s) reviewed and edited the content as needed and take(s) full responsibility for the content of the published article.


Author contributions


Alina Meyer  0009-0000-2097-6295
Conceptualization (equal), Data curation (equal), Formal analysis (equal), Investigation (equal), Methodology (equal), Project administration (equal), Software (equal), Validation (equal), Visualization (equal), Writing – original draft (equal), Writing – review & editing (equal)


Lea-Maria Mayer  0009-0007-5123-9854
Data curation (equal), Investigation (equal), Methodology (equal), Validation (equal), Writing – review & editing (equal)


Linnea Gustafsson  0000-0002-8925-2815
Conceptualization (equal), Data curation (equal), Formal analysis (equal), Investigation (equal), Methodology (equal), Software (equal), Validation (equal), Visualization (equal), Writing – review & editing (equal)


Jens Eriksson  0000-0002-8945-2665
Investigation (equal), Methodology (equal), Validation (equal), Writing – review & editing (equal)


Kathrin Klein  0000-0001-9819-2773
Investigation (equal), Validation (equal), Writing – review & editing (equal)


Florian A Büttner  0000-0002-0657-9522
Data curation (equal), Formal analysis (equal), Software (equal), Validation (equal), Writing – review & editing (equal)


Dinh Son Vo  0009-0000-4180-8231
Investigation (equal), Validation (equal), Writing – review & editing (equal)

Madlen Hubert  0000-0002-5908-9535
Funding acquisition (equal), Resources (equal), Supervision (equal), Validation (equal), Writing – review & editing (equal)

Volker M Lauschke  0000-0002-1140-6204
Funding acquisition (equal), Resources (equal), Supervision (equal), Validation (equal), Writing – review & editing (equal)

Mikael E Sellin  0000-0002-8355-0803
Funding acquisition (equal), Resources (equal), Supervision (equal), Validation (equal), Writing – review & editing (equal)

My Hedhammar  0000-0003-0140-419X
Conceptualization (equal), Funding acquisition (equal), Resources (equal), Supervision (equal), Validation (equal), Writing – review & editing (equal)

Per Artursson  0000-0002-3708-7395
Conceptualization (equal), Funding acquisition (equal), Methodology (equal), Project administration (equal), Resources (equal), Supervision (equal), Validation (equal), Visualization (equal), Writing – original draft (equal), Writing – review & editing (equal)

References

- [1] Artursson P and Karlsson J 1991 Correlation between oral drug absorption in humans and apparent drug permeability coefficients in human intestinal epithelial (Caco-2) cells *Biochem. Biophys. Res. Commun.* **175** 880–5
- [2] Hubatsch I, Ragnarsson E G E and Artursson P 2007 Determination of drug permeability and prediction of drug absorption in Caco-2 monolayers *Nat. Protocols* **2** 2111–9
- [3] Nasiri R et al 2025 Engineering biomimetic tissue barrier models on chips: from design and fabrication to applications in disease modeling and drug screening *Biomaterials* **327** 123739
- [4] Piossek F, Beneke S, Schlichenmaier N, Mucic G, Drewitz S and Dietrich D R 2022 Physiological oxygen and co-culture with human fibroblasts facilitate *in vivo*-like properties in

- human renal proximal tubular epithelial cells *Chem. Biol. Interact.* **361** 109959
- [5] Chung H H, Mireles M, Kwarta B J and Gaborski T R 2018 Use of porous membranes in tissue barrier and co-culture models *Lab Chip* **18** 1671–89
- [6] Paulsson M 1992 Basement membrane proteins: structure, assembly, and cellular interactions *Crit. Rev. Biochem. Mol. Biol.* **27** 93–127
- [7] Klein G, Langerer M, Timpl R and Ekblom P 1988 Role of laminin a chain in the development of epithelial cell polarity *Cell* **55** 331–41
- [8] Gustafsson L, Tasiopoulos C P, Jansson R, Kvick M, Duursma T, Gasser T C, van der Wijngaart W and Hedhammar M 2020 Recombinant spider silk forms tough and elastic nanomembranes that are protein-permeable and support cell attachment and growth *Adv. Funct. Mater.* **30** 2002982
- [9] Hedhammar M, Rising A, Grip S, Martinez A S, Nordling K, Casals C, Stark M and Johansson J 2008 Structural properties of recombinant nonrepetitive and repetitive parts of major ampullate spidroin 1 from *euprostenops australis*: implications for fiber formation *Biochemistry* **47** 3407–17
- [10] Widhe M, Shalaly N D and Hedhammar M 2016 A fibronectin mimetic motif improves integrin mediated cell binding to recombinant spider silk matrices *Biomaterials* **74** 256–66
- [11] Tasiopoulos C P, Gustafsson L, Van Der Wijngaart W and Hedhammar M 2021 Fibrillar nanomembranes of recombinant spider silk protein support cell co-culture in an *in vitro* blood vessel wall model *ACS Biomater. Sci. Eng.* **7** 3332–9
- [12] Karimi A and Shojaei A 2017 Measurement of the mechanical properties of the human kidney *IRBM* **38** 292–7
- [13] Gustafsson L, Gkouma S, Jönsson A, Dufva M and Hedhammar M 2024 Nanofibrillar basement membrane mimic made of recombinant functionalized spider silk in custom-made tissue culture inserts *J. Vis. Exp.* **213** 1–15
- [14] Gkouma S et al 2024 Standalone single- and bi-layered human skin 3D models supported by recombinant silk feature native spatial organization *Biofabrication* **17** 015015
- [15] Hjelm L C, Hedhammar M and Löfblom J 2023 *In vitro* blood–brain barrier model based on recombinant spider silk protein nanomembranes for evaluation of transcytosis capability of biomolecules *Biochem. Biophys. Res. Commun.* **669** 77–84
- [16] Wieser M, Stadler G, Jennings P, Streubel B, Pfäller W, Ambros P, Riedl C, Katinger H, Grillari J and Grillari-Voglauer R 2008 hTERT alone immortalizes epithelial cells of renal proximal tubules without changing their functional characteristics *Am. J. Physiol. Renal. Physiol.* **295** F1365–75
- [17] Wilmes A, Aschauer L, Limonciel A, Pfäller W and Jennings P 2014 Evidence for a role of claudin 2 as a proximal tubular stress responsive paracellular water channel *Toxicol. Appl. Pharmacol.* **279** 163–72
- [18] Aschauer L, Carta G, Vogelsang N, Schlatter E and Jennings P 2015 Expression of xenobiotic transporters in the human renal proximal tubule cell line RPTEC/TERT1 *Toxicol. Vitro* **30** 95–105
- [19] Secker P F, Schlichenmaier N, Beilmann M, Deschl U and Dietrich D R 2019 Functional transepithelial transport measurements to detect nephrotoxicity *in vitro* using the RPTEC/TERT1 cell line *Arch. Toxicol.* **93** 1965–78
- [20] Wilmes A et al 2015 Mechanism of cisplatin proximal tubule toxicity revealed by integrating transcriptomics, proteomics, metabolomics and biokinetics *Toxicol. Vitro* **30** 117–27
- [21] Vidal Yucha S E et al 2022 3D, human renal proximal tubule (RPTEC-TERT1) organoids ‘tubuloids’ for translatable evaluation of nephrotoxins in high-throughput *PLoS One* **17** e0277937
- [22] Aschauer L, Limonciel A, Wilmes A, Stanzel S, Kopp-Schneider A, Hewitt P, Lukas A, Leonard M O, Pfäller W and Jennings P 2015 Application of RPTEC/TERT1 cells for investigation of repeat dose nephrotoxicity: a transcriptomic study *Toxicol. Vitro* **30** 106–16
- [23] Bastek H, Zubel T, Stemmer K, Mangerich A, Beneke S and Dietrich D R 2019 Comparison of aristolochic acid I derived DNA adduct levels in human renal toxicity models *Toxicology* **420** 29–38
- [24] Secker P F, Luks L, Schlichenmaier N and Dietrich D R 2018 RPTEC/TERT1 cells form highly differentiated tubules when cultured in a 3D matrix *ALTEX* **35** 223–34
- [25] Meijer T et al 2025 Transcriptomic changes and mitochondrial toxicity in response to acute and repeat dose treatment with brequinar in human liver and kidney *in vitro* models *Toxicol. Vitro* **104** 106010
- [26] Meyer A, Sotiropoulou P, Bouker K, Svedberg D, Hammar R, Bange H, Larsson P, Mateus A, Dietrich D R and Artursson P 2026 Identification of drug repurposing candidates for the treatment of polycystic kidney disease Unpublished
- [27] Ewels P A, Peltzer A, Fillinger S, Patel H, Alneberg J, Wilm A, Garcia M U, Di Tommaso P and Nahnsen S 2020 The nf-core framework for community-curated bioinformatics pipelines *Nat. Biotechnol.* **38** 276–8
- [28] Edgar R, Domrachev M and Lash A E 2002 Gene expression omnibus: NCBI gene expression and hybridization array data repository *Nucleic Acids Res.* **30** 207–10
- [29] Love M I, Huber W and Anders S 2014 Moderated estimation of fold change and dispersion for RNA-seq data with DESeq2 *Genome Biol.* **15** 550
- [30] Wu T et al 2021 clusterProfiler 4.0: a universal enrichment tool for interpreting omics data *Innovation* **2** 100141
- [31] Newman A M et al 2019 Determining cell type abundance and expression from bulk tissues with digital cytometry *Nat. Biotechnol.* **37** 773–82
- [32] Kos V M et al 2025 The intracellular free concentration of endocrine disrupting chemicals enables translation between cell-free and cell-based estrogenic activity assays *Environ. Toxicol. Pharmacol.* **117** 104750
- [33] Karlsson J and Artursson P 1991 A method for the determination of cellular permeability coefficients and aqueous boundary layer thickness in monolayers of intestinal epithelial (Caco-2) cells grown in permeable filter chambers *Int. J. Pharm.* **71** 55–64
- [34] Ahlin G, Karlsson J, Pedersen J M, Gustavsson L, Larsson R, Mattsson P, Norinder U, Bergström C A S and Artursson P 2008 Structural requirements for drug inhibition of the liver specific human organic cation transport protein 1 *J. Med. Chem.* **51** 5932–42
- [35] Sandoval P J, Zorn K M, Clark A M, Ekins S and Wright S H 2018 Assessment of substrate-dependent ligand interactions at the organic cation transporter OCT2 using six model substrates *Mol. Pharmacol.* **94** 1057–68
- [36] Lepist E-I et al 2014 Contribution of the organic anion transporter OAT2 to the renal active tubular secretion of creatinine and mechanism for serum creatinine elevations caused by cobicistat *Kidney Int.* **86** 350–7
- [37] Sziráki I et al 2011 Quinidine as an ABCB1 probe for testing drug interactions at the blood–brain barrier *an in vitro in vivo* correlation study SLAS discovery *J. Biomol. Screen* **16** 886–94
- [38] Meyer A, Khalil B, Iljin M, Bange H, Price L S, Dyubankova N, van Westen G J P, van Vlijmen H, Peters D J M and Artursson P 2025 A patient-derived 3D cyst model of polycystic kidney disease that mimics disease development and responds to repurposing candidates *Clin. Transl. Sci.* **18** e70214
- [39] Miner J H 1999 Renal basement membrane components *Kidney Int.* **56** 2016–24
- [40] Soltoff S P 1986 ATP and the regulation of renal cell function *Annu. Rev. Physiol.* **48** 9–31
- [41] Gusnard D and Kirschner R H 1977 Cell and organelle shrinkage during preparation for scanning electron microscopy: effects of fixation, dehydration and critical point drying *J. Microsc.* **110** 51–57

- [42] Homan K A, Kolesky D B, Skylar-Scott M A, Herrmann J, Obuobi H, Moisan A and Lewis J A 2016 Bioprinting of 3D convoluted renal proximal tubules on perfusable chips *Sci. Rep.* **6** 34845
- [43] Chandrasekaran V et al 2021 Generation and characterization of iPSC-derived renal proximal tubule-like cells with extended stability *Sci. Rep.* **11** 11575
- [44] Yang C Z, Yaniger S I, Jordan V C, Klein D J and Bittner G D 2011 Most plastic products release estrogenic chemicals: a potential health problem that can be solved *Environ. Health Perspect.* **119** 989–96
- [45] Galetin A et al 2024 Membrane transporters in drug development and as determinants of precision medicine *Nat. Rev. Drug Discovery* **23** 255–80
- [46] Tsang Y P, Rodriguez A G, Warren M S and Unadkat J D 2025 Identification of selective substrates and inhibitors of the major human renal uptake transporters *Drug Metab. Dispos.* **53** 100046
- [47] Renkin E M 1954 Filtration, diffusion, and molecular sieving through porous cellulose membranes *J. Gen. Physiol.* **38** 225–43
- [48] Kaissling B and Le Hir M 2008 The renal cortical interstitium: morphological and functional aspects *Histochem. Cell Biol.* **130** 247–62
- [49] Sonavane M 2022 Classical and non-classical estrogen receptor effects of bisphenol A *Bisphenol A: A Multi-Modal Endocrine Disruptor (Issues in Toxicology)* ed N R Gassman (The Royal Society of Chemistry) pp 1–25
- [50] Krause G, Winkler L, Mueller S L, Haseloff R F, Piontek J and Blasig I E 2008 Structure and function of claudins *Biochim. Biophys. Acta* **1778** 631–45
- [51] Meijer T, da Costa Pereira D, Klatt O C, Buitenhuis J, Jennings P and Wilmes A 2024 Characterization of organic anion and cation transport in three human renal proximal tubular epithelial models *Cells* **13** 1008
- [52] King S M et al 2017 3D proximal tubule tissues recapitulate key aspects of renal physiology to enable nephrotoxicity testing *Front. Physiol.* **8** 123
- [53] Specioso G et al 2022 Apical medium flow influences the morphology and physiology of human proximal tubular cells in a microphysiological system *Bioengineering* **9** 516
- [54] Jang K-J, Mehr A P, Hamilton G A, McPartlin L A, Chung S, Suh K-Y and Ingber D E 2013 Human kidney proximal tubule-on-a-chip for drug transport and nephrotoxicity assessment *Integr. Biol.* **5** 1119–29
- [55] ICH M12 Guideline on drug interaction studies 2024 (available at: <https://www.ema.europa.eu/en/ich-m12-drug-interaction-studies-scientific-guideline#current-version-67814>)
- [56] Källén A, Taebnia N, Widhe M, Lauschke V M and Hedhammar M 2025 3D culture in functionalized fn-silk networks facilitate proliferation, differentiation and phenotypic stability of mature human primary cells and stem cells *Biotechnol. Bioeng.* **122** 2522–34
- [57] ColloDET C, Blust K, Gkouma S, Ståhl E, Chen X, Hartman J and Hedhammar M 2023 Development and characterization of a recombinant silk network for 3D culture of immortalized and fresh tumor-derived breast cancer cells *Bioeng. Transl. Med.* **8** e10537